

## Phosphorus Abundances of B-Type Stars in the Solar Neighborhood

Yoichi Takeda

11-2 Enomachi, Naka-ku, Hiroshima-shi, Japan 730-0851

e-mail: ytakeda@js2.so-net.ne.jp

*Received Month Day, Year*

### ABSTRACT

Phosphorus abundances of  $\sim 80$  apparently bright sharp-lined early-to-late B-type stars on the upper main sequence are determined by applying the non-LTE analysis to the P II line at 6043.084 Å, with an aim of getting information on the P abundance of the galactic gas (from which these young stars were formed) in comparison with the reference solar abundance ( $A_{\odot} \simeq 5.45$ ). These sample stars turned out to be divided into two distinct groups with respect to their P abundances: (1) chemically peculiar late B-type stars of HgMn group show considerable overabundances of P (supersolar by  $\sim 0.5$ – $1.5$  dex), the extent of which progressively increases with  $T_{\text{eff}}$ . (2) In contrast, the P abundances of normal B-type stars are comparatively homogeneous, though a notable difference is observed between the LTE and non-LTE cases. Although their LTE abundances are near-solar, a slight gradual trend with  $T_{\text{eff}}$  is observed. However, after applying the negative non-LTE corrections (amounting  $\sim 0.1$ – $0.5$  dex), this  $T_{\text{eff}}$ -dependence is successfully removed, but the resulting non-LTE abundances (their mean is  $\simeq 5.20$ ) are appreciably underabundant relative to the Sun by  $\sim 0.2$ – $0.3$  dex. The cause of this systematic discrepancy (contradicting the galactic chemical evolution) is yet to be investigated.

**Key words:** *Galaxy: solar neighborhood – stars: abundances – stars: chemically peculiar – stars: early-type – stars: population I*

### 1. Introduction

Astrophysical interest in the cosmic abundance of phosphorus (P;  $Z = 15$ ) is rapidly growing these days. While one reason is that the mechanism of how this element is synthesized in the chemical evolution of the Galaxy is not yet well understood, another intriguing motivation lies in its astrobiological context. That is, P is (along with H, C, N, O) an indispensable key element for life, which is the backbone of nuclear acids (RNA, DNA) or cell membranes, and plays a significant role in producing/reserving the vital energy via ATP (Adenosine TriPhosphate). Especially, the original P abundance of protoplanetary material (or star-forming gas) in comparison with that of the Sun (comparatively P-rich) is an important factor, because substantially subsolar case would make it difficult to leave sufficient amount

P for life on the surface of planets due to its strongly partitioning nature in the planetary core (Hinkel et al. 2020).

Accordingly, not a few stellar spectroscopists devoted their energies to P abundance determinations since 2010s, and more than a dozen papers have been published during the short period of the past decade (see, e.g., Table 1 of Sadakane & Nishimura 2022, Sect. 1 of Maas et al. 2022, and the references therein). These authors established the phosphorus abundances of various late-type (FGK-type) stars by using neutral P I lines in the near-infrared region ( $Y$ -band or  $H$ -band) or in the ultraviolet region ( $\sim 2135 \text{ \AA}$ ).

It has thus revealed that  $[\text{P}/\text{Fe}]$  (logarithmic P-to-Fe ratio) tends to progressively increase with a decrease in the metallicity ( $[\text{Fe}/\text{H}]$ ) like  $\alpha$ -elements for stars of disk population (from  $[\text{P}/\text{Fe}] \sim 0$  at  $[\text{Fe}/\text{H}] \sim 0$  to  $[\text{P}/\text{Fe}] \sim +0.5$  at  $[\text{Fe}/\text{H}] \sim -1$ ) whereas it turns to drop again in the metallicity regime of halo population ( $[\text{P}/\text{Fe}] \sim 0$  at  $[\text{Fe}/\text{H}] \lesssim -2$ ), as shown in Fig. 1 of Bekki & Tsujimoto (2024). While several theoreticians tried to explain this trend of  $[\text{P}/\text{Fe}]$  mainly in terms of the P production by core-collapse supernovae, Bekki & Tsujimoto (2024) recently argued that oxygen–neon (ONe) novae (triggered in close binary systems including heavier white dwarfs) should play a significant role in the galactic nucleosynthesis of P.

However, these studies are directed only to comparatively cool stars of lower mass (typically around  $\sim 1M_{\odot}$ ) which have ages on the order of  $\sim 10^9$ – $10^{10}$  yr. Meanwhile, much less efforts have been made to young hotter stars, such as B-type stars of  $\sim 3$ – $10 M_{\odot}$  (reflecting the gas composition of the Galaxy in the more recent past; i.e. several times  $\sim 10^7$ – $10^8$  yr ago). Actually, phosphorus abundance determinations of B stars are generally scarce, excepting HgMn stars (chemically peculiar late B-type stars showing considerable overabundance of P by up to  $\sim 1$ – $2$  dex), for which P abundances have been reported for quite a number of stars as compiled by Ghazaryan & Alecian (2016).

This is presumably due to the difficulty in finding useful P lines of sufficient strengths. In the atmosphere of B-type stars, P atoms are mainly in the ionization stages of P II (late–mid B) or P III (early B), as illustrated in Fig. 1. Since available P II or P III lines in the optical wavelength regions are all of high-excitations ( $\chi_{\text{low}} > 10$  eV), they are fairly weak in strength for the case of usual (near-solar) P abundances and thus not easy to detect.<sup>1</sup>

As such, published studies of P abundances for “normal” B-type stars are quite limited:

- Phosphorus abundances are reported for the well-studied benchmark sharp-lined star  $\iota$  Her (B3 IV), as summarized in Table 1 of Golriz & Landstreet (2017). However, the results by three studies (Pintado & Adelman 1993; Peters & Polidan 1985; Peters & Aller 1970; based either on P II or P III

<sup>1</sup>Although strong low-excitation P II or P III lines do exist in the ultraviolet region, they are not suitable for reliable abundance determinations (i.e., too strong and apt to suffer blending).

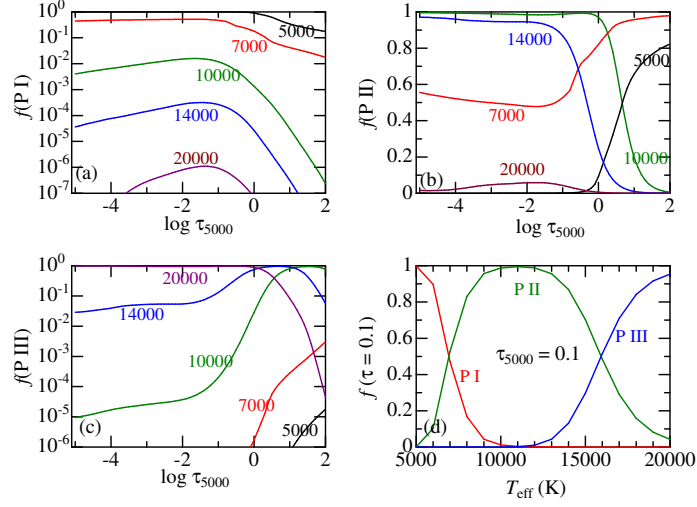


Fig. 1. Number population fraction ( $f$ ) of (a) neutral, (b) once-ionized, and (c) twice-ionized phosphorus species relative to the total P atoms [e.g.,  $f(\text{P I}) \equiv N(\text{P I})/N_{\text{total}}^{\text{P}}$ ], plotted against the continuum optical depth at 5000 Å. Calculations were done for five  $\log g = 4.0$  solar-metallicity models of different  $T_{\text{eff}}$  (5000, 7000, 10000, 14000, and 20000 K) as indicated in each panel. The runs of  $f$  (at  $\tau_{5000} = 0.1$ ) with  $T_{\text{eff}}$  for these three stages are also depicted in panel (d). All these calculations were done in LTE (use of Saha's equation).

lines) show rather large diversities in  $A^2$  from  $\sim 5.8$  to  $\sim 6.4$ ; i.e., apparently P-rich if simply compared with the solar abundance ( $A_{\odot} = 5.45$ ).<sup>3</sup>

- Pintado & Adelman (1993) also determined the P abundance of  $\gamma$  Peg (B2 IV) from P III lines to be  $A \sim 5.4$  (i.e., almost solar).
- In Allen's (1998) abundance studies on early A and late B stars, attempts of P abundance determinations for 7 normal stars based on P II lines in the optical region turned out to be unsuccessful, though 5 HgMn stars were confirmed to be significantly P-rich ( $A \sim 5.9$ –7.8).
- Fossati et al.'s (2009) analysis on 2 normal late B-type stars (21 Peg and  $\pi$  Cet) based on P II lines yielded  $[\text{P}/\text{H}]^4 \sim +0.3$  dex (moderately overabundant) for both.
- In Niemczura et al.'s (2009) abundance study on late B-type stars (including HgMn stars), the P abundances of 3 normal stars were determined as  $A =$

<sup>2</sup> $A$  is the logarithmic number abundance of the element (P) relative to that of hydrogen with the usual normalization of  $A_{\text{H}} = 12$  for H.

<sup>3</sup>In this article, Anders & Grevesse's (1989) solar photospheric P abundance of  $A_{\odot} = 5.45$  is adopted as the reference, in order to keep consistency with Kurucz's (1993) ATLAS9/WIDTH9 program. See Appendix A for a more detailed discussion on this subject.

<sup>4</sup>As usual,  $[\text{X}/\text{H}]$  is the differential abundance of element X relative to the Sun; i.e.,  $[\text{X}/\text{H}] \equiv A_{\text{star}}(\text{X}) - A_{\odot}(\text{X})$ .

6.01 (HD 49481), 5.60 (HD 50251), and 5.28 (HD 182198); i.e., nearly solar or moderately supersolar.

- Przybilla et al. (2006) derived a near-solar P abundance of  $A = 5.53(\pm 0.06)$  for the B-type supergiant  $\beta$  Ori (B8 Iae) based on 4 P II lines.

Therefore, phosphorus abundance problem of normal B-type stars is far from being settled (near-solar? or somewhat supersolar?), given such insufficient data by different investigators for only a small number of stars. What we require is a comprehensive study based on a large sample of stars, by which wealthy and homogeneous data of P abundances would be accomplished.

Motivated by this consideration, I decided to conduct an extensive analysis of P abundances for  $\sim 80$  young B-type stars (including HgMn stars) by using the P II line at 6043.08 Å (hereinafter often referred to as P II 6043; it is the strongest P II line in the optical region and almost free from any appreciable blending), in order to estimate the P composition of the galactic gas at the time of their formation.

Besides, an emphasis was placed on incorporating the non-LTE affect in P abundance determinations based on statistical equilibrium calculations. Since non-LTE calculation for P has never been carried out so far (to the author's knowledge) and all the past investigations mentioned above were done based on the assumption of LTE, it would be interesting to see how the new non-LTE results compare with the previous ones.

In addition, the significance of the non-LTE effect in the determination of phosphorus abundance in the Sun (and FGK-type stars) based on P I lines in the near-infrared region was also examined as a related topic. This supplementary analysis is separately presented in Appendix A.

## 2. Observational Data

The observational materials used in this study are the high-dispersion ( $R \sim 70000$ ) and high-S/N ( $\sim 200\text{--}700$ ) spectra obtained by High Dispersion Echelle Spectrograph (HIDES) placed at the coudé focus of the 188 cm reflector at Okayama Astrophysical Observatory, which are the same as already employed in the previous two papers of the author. (i) 64 early-to-late B-type stars (mostly normal stars but some are late-B chemically peculiar stars) observed in 2006 October, which were studied by Takeda et al. (2010; hereinafter referred to as Paper I) for their O and Ne abundance determinations by using O I 6156–8 and Ne I 6143 lines. (ii) 21 late B-type stars (HgMn-type peculiar stars and normal stars) observed in 2012 May, which were analyzed by Takeda et al. (2014; hereinafter Paper II) for their Na abundance determinations based on Na I 5890/5896 lines. See these original papers for more details about the adopted spectra. The program stars (85 in total) are all sufficiently sharp-lined (projected rotational velocities are  $v_e \sin i \lesssim 60 \text{ km s}^{-1}$ ) and are located in the solar neighborhood (within  $\lesssim 1 \text{ kpc}$ ). Their fundamental stellar data are listed in Table 1, where two groups (i) and (ii) are presented separately.

These 85 targets are plotted on the  $\log L$  vs.  $\log T_{\text{eff}}$  diagram in Fig. 2, where Lejeune & Schaerer’s (2001) standard theoretical evolutionary tracks (solar metallicity, non-rotating models with mass loss; see Sect. 2 therein for the details of the input physics they adopted) corresponding to different stellar masses are also depicted. This figure indicates that the sample stars are in the mass range of  $2.5M_{\odot} \lesssim M \lesssim 9M_{\odot}$ .

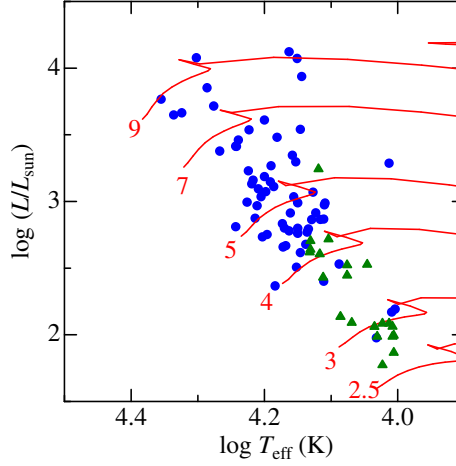


Fig. 2. Plots of 85 program stars on the theoretical HR diagram ( $\log(L/L_{\odot})$  vs.  $\log T_{\text{eff}}$ ), where blue filled circles and green filled triangles correspond to 64 stars of 2006 October observations and 21 stars of 2012 May observations, respectively. Theoretical evolutionary tracks of solar metallicity stars for six different initial masses (2.5, 3, 4, 5, 7, and  $9 M_{\odot}$ ), which were computed by Lejeune & Schaerer (2001), are also depicted by red lines for comparison. See Sect. 3 for the adopted  $T_{\text{eff}}$ , and the caption of Fig. 1 in Paper I (or Paper II) regarding how  $L$  was evaluated.

### 3. Atmospheric Parameters

Regarding the effective temperature ( $T_{\text{eff}}$ ) and the surface gravity ( $\log g$ ) of each star, the same values as adopted in Papers I and II are used unchanged (cf. Table 1), which were determined from colors ( $b-y$ ,  $c_1$ ,  $m_1$ , and  $\beta$ ) of Strömgren’s  $uvby\beta$  photometric system.

As to the microturbulence ( $\xi$ ), the values assumed in Paper I [ $3(\pm 2)$  km s $^{-1}$  for early-to-late B-type stars] and Paper II [ $1(\pm 1)$  km s $^{-1}$  for late B-type stars] were not consistent. In this paper,  $T_{\text{eff}}$ -dependent values are assigned as  $\xi = 1(\pm 1)$  km s $^{-1}$  ( $10000 \text{ K} < T_{\text{eff}} < 16500 \text{ K}$ ) and  $\xi = 2(\pm 1)$  km s $^{-1}$  ( $16500 \text{ K} < T_{\text{eff}} < 23000 \text{ K}$ ).

This is due to the fact that  $\xi$  plays a significant role only for the case of P-rich chemically peculiar stars (HgMn stars) found only among late B-type stars, while the P-line strengths of normal stars (existing over the entire  $T_{\text{eff}}$  range) are so weak that their P abundances are practically  $\xi$ -independent. Therefore, the same value as in Paper II ( $\xi = 1$  km s $^{-1}$ ; specific to late B-type stars) is adopted for

$T_{\text{eff}} < 16500$  K. while a tentative value of  $2 \text{ km s}^{-1}$  is roughly assumed at  $T_{\text{eff}} > 16500$  K (all are normal stars with weak lines of phosphorus).

The model atmospheres adopted for each of the targets are the same as in Papers I and II, which are the solar-metallicity models constructed by two-dimensionally interpolating Kurucz's (1993) ATLAS9 model grid in terms of  $T_{\text{eff}}$  and  $\log g$ .

#### 4. Spectrum Fitting Analysis and Evaluation of Equivalent Widths

As already mentioned in Sect. 1, it is important to employ a spectral line of as large transition probability ( $\log gf$ ) as possible for successful P abundance determinations of B-type stars, because lines tend to be considerably weak and hard to detect for near-normal P abundances. In this respect, the suitable candidate lines in the optical region are the P II lines of  $4s^3P^{\circ} - 4p^3D$  transition (lower excitation potentials of  $\chi_{\text{low}} \sim 10.8 \text{ eV}$ , multiplet 5). They are at 6024.13, 6034.34, 6043.08, 6087.84, and 6165.60 Å and have  $\log gf$  values of +0.20, -0.15, +0.44, -0.38, and -0.41, respectively, according to the VALD database (Ryabchikova et al. 2015). Therefore, we invoke the P II line at 6043.08 Å, which is the strongest one among these and also free from any appreciable blending. Besides, this line has another advantage that it lies almost in the middle part of the relevant Echelle order (covering 5990–6100 Å) where the S/N ratio is comparatively higher.

The procedures of analysis (spectrum fitting, equivalent width derivation, estimating abundance errors due to parameter uncertainties) are essentially the same as adopted in Papers I and II (cf. Sect. 4 therein). Note that all the calculations in this section are done with the assumption of LTE at this stage.

##### 4.1. Synthetic Spectrum Fitting

First, a spectrum-fitting technique was applied to the 6040–6050 Å region (comprising the P II 6043 line), by which the best-fit between theoretical and observed spectra is accomplished. Here, the parameters varied are the abundances of P, O, and Ne (+ Mn if necessary), rotational broadening velocity ( $v_e \sin i$ ), and radial velocity ( $V_{\text{rad}}$ ). The data of all atomic lines included in this wavelength region were taken from the VALD database (Ryabchikova et al. 2015). Specifically, the data for the relevant P II line at 6043.084 Å are  $\chi_{\text{low}} = 10.802 \text{ eV}$  (lower excitation potential),  $\log gf = +0.442$  (logarithmic  $gf$  value),  $\text{Gammar} = 9.22$  (radiation damping parameter),  $\text{Gammas} = -5.76$  (Stark effect damping parameter), and  $\text{Gammaw} = -7.73$  (van der Waals effect damping parameter).<sup>5</sup> The phosphorus abundances could be successfully established for 83 stars (out of 85 program stars), except for HD 029248 and HR 3652, for which the P abundance was tentatively fixed at an arbitrary value in the fitting. The agreement between the theoretical spectrum (for

<sup>5</sup> $\text{Gammar}$  is the radiation damping width ( $\text{s}^{-1}$ ),  $\log \gamma_{\text{rad}}$ .  $\text{Gammas}$  is the Stark damping width ( $\text{s}^{-1}$ ) per electron density ( $\text{cm}^{-3}$ ) at  $10^4$  K,  $\log(\gamma_e/N_e)$ .  $\text{Gammaw}$  is the van der Waals damping width ( $\text{s}^{-1}$ ) per hydrogen density ( $\text{cm}^{-3}$ ) at  $10^4$  K,  $\log(\gamma_w/N_H)$ .

the solutions with converged parameters) with the observed spectrum for each star is shown in Fig. 3.

#### 4.2. Equivalent Widths and Their Errors

Next, the equivalent width of the P II 6043 line  $W_{6043}$  was inversely evaluated from the abundance solution resulting from the fitting analysis. The  $W_{6043}$  values derived in this manner are given in Table 1. While this line is generally weak for ordinary B stars ( $1 \text{ m}\text{\AA} \lesssim W_{6043} \lesssim 10 \text{ m}\text{\AA}$ ), it can be stronger (up to  $W_{6043} \sim 100 \text{ m}\text{\AA}$ ) for P-rich peculiar stars (cf. Fig. 4a).

The error involved with  $W_{6043}$  was estimated as

$$\delta W \sim \epsilon W_{6043}(1 - R_0)/R_0 \quad (1)$$

according to Takeda (2023; cf. Sect. 6.2 therein) where  $\epsilon (\equiv (S/N)^{-1})$  is the random fluctuation of the continuum level and  $R_0 (\equiv 1 - F_0/F_c)$  is the line depth at the line center. By inserting the S/N ratios (measured around the P II 6043 line; see column 12 in Table 1) into Eq. (1), typical values of  $\delta W$  were found to be  $\sim 1\text{--}3 \text{ m}\text{\AA}$  in most cases<sup>6</sup> (or up to  $\sim 10 \text{ m}\text{\AA}$  in the exceptional case of low S/N and very shallow  $R_0$ ), as depicted by error bars attached to the symbols in Fig. 4a. The impact of  $\delta W$  on the P abundance (denoted as  $\delta_W$ ) can be significant (e.g., a few tenths dex or even more) for the very weak line case where  $W_{6043}$  and  $\delta W$  are on the similar size.

#### 4.3. Impact of Parameter Uncertainties

How the ambiguities in atmospheric parameters ( $T_{\text{eff}}$ ,  $\log g$ , and  $\xi$ ) affect the P abundances was estimated by repeating the analysis on the  $W_{6043}$  values while perturbing these standard parameters interchangeably by  $\pm 3\%$ ,  $\pm 0.2$  dex, and  $\pm 1 \text{ km s}^{-1}$ , which are the typical uncertainties for  $T_{\text{eff}}$  and  $\log g$  (cf. Sect. 3 in Paper I) and for  $\xi$  (cf. Sect. 3 of this paper).

The resulting  $A^{\text{L}}$  (P abundances in LTE),  $\delta_{T\pm}$  (abundance changes by perturbations of  $T_{\text{eff}}$ ),  $\delta_{g\pm}$  (abundance changes by perturbations of  $\log g$ ), and  $\delta_{\xi\pm}$  (abundance changes by perturbations of  $\xi$ ) are plotted against  $T_{\text{eff}}$  in Figs. 4b, 4c, 4d, and 4e, respectively.

As seen from Figs. 4c and 4d, both  $|\delta_T|$  and  $|\delta_g|$  are  $\lesssim 0.1$  dex and thus not very significant. According to Fig. 4e,  $|\delta_{\xi}|$  is negligibly small for normal stars, while  $|\delta_{\xi}|$  amounts up to  $\sim 0.1$  dex for P-rich late B-type peculiar stars. The error bars attached to the symbols in Fig. 4b are the root-sum-squares of  $\delta_W$ ,  $\delta_T$ ,  $\delta_g$ , and  $\delta_{\xi}$ .

<sup>6</sup>Errors of  $W_{6043}$  evaluated by Cayrel's (1988) formula (depending on S/N, pixel size, and line widths) were found to be smaller (typically by several times) than  $\delta W$  defined by Eq. (1), and thus not taken into account.

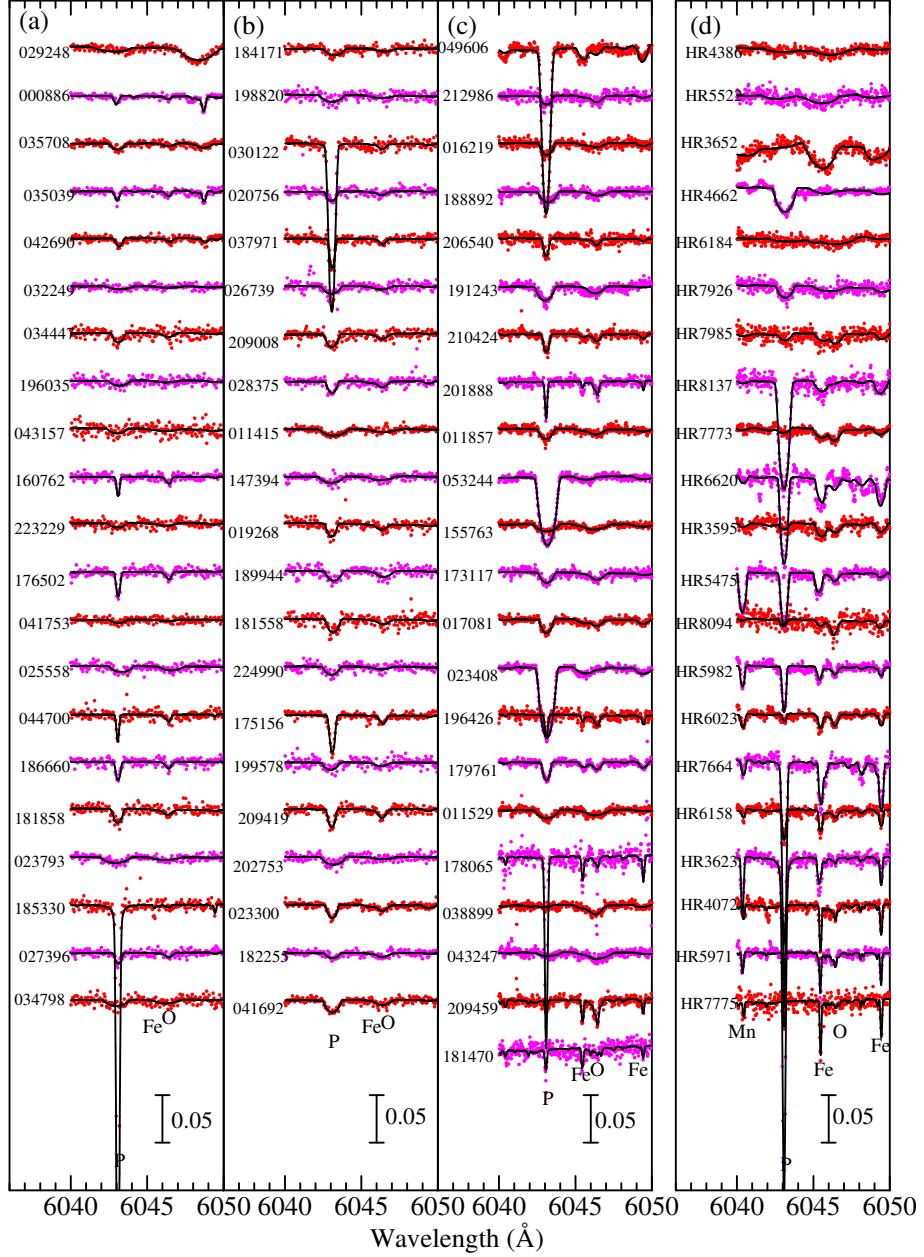


Fig. 3. Synthetic spectrum fitting at the 6040–6050 Å region for the determination of P abundances. The best-fit theoretical spectra are depicted by solid lines, while the observed data are plotted by dots. The spectra are arranged in the same manner as in Table 1: Panels (a), (b), and (c) are for the 64 early-to-late B stars of 2006 October observations (indicated by the HD number) in the descending order of  $T_{\text{eff}}$  (from top to bottom; from left to right). while the rightmost panel (d) is for 21 late-B stars of 2012 May observations (indicated by the HR number) in the descending order of  $v_e \sin i$ . An offset of 0.05 (in unit of the continuum-normalized flux) is applied to each spectrum relative to the adjacent one.



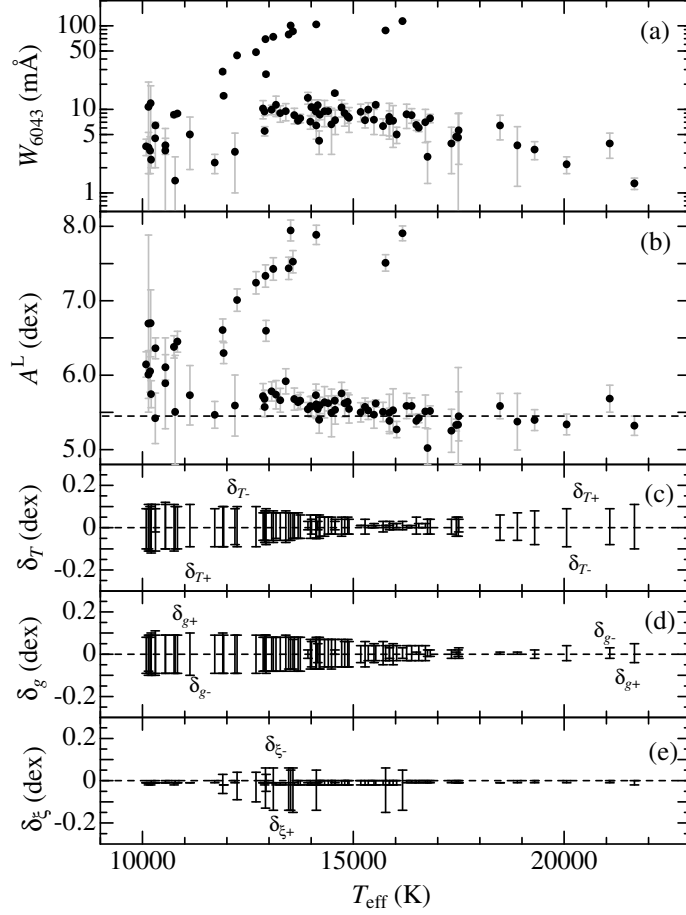


Fig. 4. The equivalent widths of the P II 6043 line, resulting LTE abundances, and sensitivities due to perturbations of atmospheric parameters, are plotted against  $T_{\text{eff}}$ . (a)  $W_{6043}$  (equivalent width), where the indicated error bars ( $\delta W$ ) are their uncertainties (see Sect. 4.2 for more details). (b)  $A^L$  (LTE phosphorus abundance). Here, the attached error bars are the root-sum-squares of  $\delta W$  (abundance ambiguities corresponding to  $\delta W$ ),  $\delta_T$ ,  $\delta_g$ , and  $\delta_\xi$ . (c)  $\delta_{T+}$  and  $\delta_{T-}$  (abundance variations in response to  $T_{\text{eff}}$  changes of +3% and -3%). (d)  $\delta_{g+}$  and  $\delta_{g-}$  (abundance variations in response to  $\log g$  changes of +0.2 dex and -0.2 dex). (e)  $\delta_{\xi+}$  and  $\delta_{\xi-}$  (abundance variations in response to perturbing the standard  $\xi$  value by  $\pm 1 \text{ km s}^{-1}$ ). Note that the signs of  $\delta_T$  and  $\delta_g$  are reversed on both sides of  $T_{\text{eff}}$  around  $\sim 16000\text{--}18000 \text{ K}$  (mid B-type).

## 5. Statistical Equilibrium Calculations for P II

### 5.1. Atomic Model

The non-LTE calculations for P II were carried out based on the P II model atom comprising 83 terms (up to  $3s^2 3p 9g$  at  $154582 \text{ cm}^{-1}$ ) and 1206 radiative transitions, which was constructed by consulting the updated atomic line data (filename: “gfall21oct16.dat”)<sup>7</sup> compiled by Dr. R. L. Kurucz. Though the contribution of P I

<sup>7</sup><http://kurucz.harvard.edu/linelists/gfnew/>

was neglected, P III was taken into account in the number conservation of total P atoms.

Regarding the photoionization cross section, the data calculated by Nahar et al. (2017)<sup>8</sup> were used for the lowest 4 terms (<sup>3</sup>P, <sup>1</sup>D, <sup>1</sup>S, and <sup>5</sup>S<sup>o</sup>), while the hydrogenic approximation was assumed for the remaining terms. Otherwise (such as the treatment of collisional rates), the recipe described in Sect. 3.1.3 of Takeda (1991) was followed (inelastic collisions due to neutral hydrogen atoms were formally included as described therein, though insignificant in the atmosphere of early-type stars considered here).

### 5.2. Grid of Models

The calculations were done on a grid of 36 ( $= 9 \times 4$ ) solar-metallicity model atmospheres resulting from combinations of nine  $T_{\text{eff}}$  values (9000, 10000, 12000, 14000, 16000, 18000, 20000, 22000, and 24000 K) and four  $\log g$  values (3.0, 3.5, 4.0, and 4.5) while assuming  $\xi = 2 \text{ km s}^{-1}$ . Regarding the input P abundance, three values of  $A(\text{P}) = 4.45, 5.45, \text{ and } 6.45$  (corresponding to  $[\text{P}/\text{H}] = -1, 0, \text{ and } +1$ ) were assumed, resulting in three kinds of non-LTE grids. The depth-dependent non-LTE departure coefficients to be used for each star were then evaluated by interpolating the grid (for each  $[\text{P}/\text{H}]$ ) in terms of  $T_{\text{eff}}$  and  $\log g$ .

## 6. Non-LTE Effect on P Abundance Determinations

### 6.1. Characteristic Trends

Fig. 5 displays the  $l_0^{\text{NLTE}}(\tau)/l_0^{\text{LTE}}(\tau)$  (the non-LTE-to-LTE line-center opacity ratio; almost equal to  $\simeq b_1$ ) and  $S_L(\tau)/B(\tau)$  (the ratio of the line source function to the Planck function; nearly equal to  $\simeq b_u/b_1$ ) for the transition relevant to the P II 6043 line ( $b_l$  and  $b_u$  are the non-LTE departure coefficients for the lower and upper levels) as functions of optical depth at  $5000\text{\AA}$  for selected representative cases. Likewise, Fig. 6 illustrates how the theoretical equivalent widths calculated in LTE ( $W^L$ ) as well as in non-LTE ( $W^N$ ) and the corresponding non-LTE corrections ( $\Delta \equiv A^N - A^L$ , where  $A^L$  and  $A^N$  are the abundances derived from  $W^N$  with LTE and non-LTE) depend upon  $T_{\text{eff}}$ . The following characteristic trends are read from these figures.

- As seen from Fig. 6, the inequality  $W^N > W^L$  (and  $\Delta < 0$ ) holds in most cases (except for the high  $T_{\text{eff}}$  end at  $\gtrsim 20000 \text{ K}$  where the trend is inverse), which means that the non-LTE effect tends to strengthen the P II 6043 line.
- For a given  $[\text{P}/\text{H}]$ ,  $|\Delta|$  almost correlates with  $W$  as well as  $T_{\text{eff}}$  in the sense that  $|\Delta|$  takes the largest value around  $T_{\text{eff}} \sim 15000 \text{ K}$  where  $W$  reaches a

<sup>8</sup>The cross-section profiles (as functions of ionizing photon energy) were roughly digitized from their Fig. 1, where attention was paid to reproduce only the global trend, because many sharp resonance peaks included in the original data are very difficult to read out.

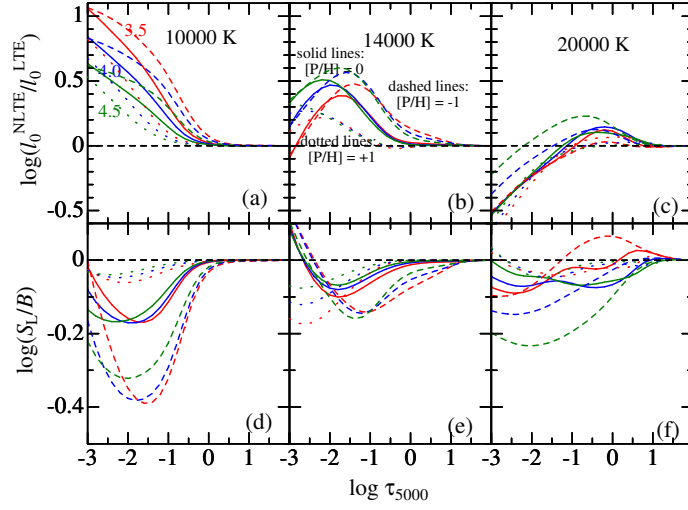


Fig. 5. The non-LTE-to-LTE line-center opacity ratio (upper panels (a)–(c)) and the ratio of the line source function ( $S_L$ ) to the local Planck function ( $B$ ) (lower panels (d)–(f)) for the P II  $4s^3P^{\circ} - 4p^3D$  transition (corresponding to P II 6043.08 line) of multiplet 5, plotted against the continuum optical depth at 5000 Å. Shown here are the calculations done with  $\xi = 2 \text{ km s}^{-1}$  on the solar-metallicity models of  $T_{\text{eff}} = 10000 \text{ K}$  (left panels (a), (d)), 14000 K (middle panels (b), (e)), and 20000 K (right panels (c), (f)). At each panel, the results for three different P abundances ( $[P/H] = -1, 0, \text{ and } +1$ ) are discriminated by line-types (dashed, solid, and dotted lines, respectively), while those for three  $\log g$  values of 3.5, 4.0, and 4.5 are depicted by different colors (red, blue, and green, respectively).

maximum, as recognized from each panel of Fig. 6. This is understandable because an increase of  $W$  makes the line formation zone shallower where the departure from LTE is larger.

- As to  $g$ -dependence of the non-LTE effect,  $|\Delta|$  tends to be larger for lower  $\log g$  (i.e., lower density atmosphere) as seen at  $T_{\text{eff}} \lesssim 15000 \text{ K}$ , though the situation is not so simple at the higher  $T_{\text{eff}}$  regime where  $\Delta$  gradually shifts in the direction of changing its sign.
- A more important factor significantly affecting the degree of departure from LTE is the P abundance ( $[P/H]$ ) assumed in the calculations. That is, the non-LTE effect ( $|\Delta|$ ) tends to be progressively less significant with an increase in  $[P/H]$  (Fig. 6d  $\rightarrow$  Fig. 6e  $\rightarrow$  Fig. 6f) if compared at the same  $T_{\text{eff}}$  and  $\log g$ , despite that the line strength ( $W$ ) is enhanced with increasing  $[P/H]$  (Fig. 6a  $\rightarrow$  Fig. 6b  $\rightarrow$  Fig. 6c).
- This  $[P/H]$ -dependence may be understood by considering the mechanism controlling the level populations for the relevant P II 6043 line. The lower level ( $4s^3P^{\circ}$ ;  $\chi_{\text{low}} \simeq 10.8 \text{ eV}$ ) of this transition is radiatively connected to the ground level ( $3p^2^3P$ ;  $\chi_{\text{low}} \simeq 0 \text{ eV}$ ) by lines of large transition probabilities at  $\sim 1150\text{--}1160 \text{ \AA}$ . Then, this strong UV transition is almost in the condition of radiative detailed balance (if it is sufficiently optically thick),

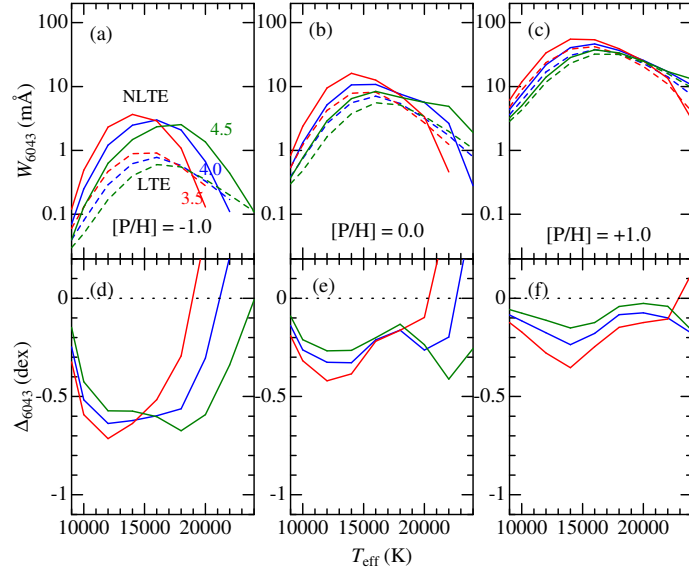


Fig. 6. The non-LTE and LTE equivalent widths ( $W^N$  and  $W^L$ ) for the P II 6043 line and the corresponding non-LTE corrections ( $\Delta \equiv A^N - A^L$ , where  $A^L$  and  $A^N$  are the abundances derived from  $W^N$  with LTE and non-LTE), which were computed on the non-LTE grid of models described in Sect. 5.2, are plotted against  $T_{\text{eff}}$ . The upper panels ((a)–(c)) are for  $W^N$  (solid lines) and  $W^L$  (dashed lines), while the lower panels ((d)–(f)) are for  $\Delta$ . The left ((a), (d)), middle ((b), (e)), and right ((c), (f)) panels correspond to  $[P/H] = -1, 0, \text{ and } +1$ , respectively. In each panel, the results for different  $\log g$  (3.5, 4.0, and 4.5) are depicted in different colors (red, blue, and green, respectively),

which makes the  $4s \ ^3P^\circ$  level as if “meta-stable”. In this case, if the subordinate lines originating from  $4s \ ^3P^\circ$  become optically thin, this level would be overpopulated ( $b > 1$ ) by cascading from the upper levels. Here, the P abundance would play a significant role in the sense that lower  $[P/H]$  (thinner optical thickness of subordinate lines) leads to more enhanced cascades and larger overpopulation. Actually, the extent of overpopulation systematically increases with a decrease in  $[P/H]$  if compared at the same depth (dotted lines  $\rightarrow$  solid lines  $\rightarrow$  dashed lines in Fig. 5a–5c).

- Note, however, that this argument is based on the presumption that the  $3p^2 \ ^3P - 4s \ ^3P^\circ$  UV transition is so optically thick to be in detailed balancing. This condition is destined to break down when double ionization proceeds and P II is replaced by P III ( $T_{\text{eff}} \gtrsim 16000$  K; cf. Fig. 1d), because the population of P II ground level comes short due to ionization. In this case, the  $4s \ ^3P^\circ$  level can not be meta-stable any more, and eventually becomes underpopulated ( $b < 1$ ). Figs. 5a–5c illustrate this situation of how the overpopulation progressively turns into underpopulation in the optically-thin layer as  $T_{\text{eff}}$  increases from late B to early B. This also explains the reason why  $\Delta$  becomes positive (i.e., non-LTE line weakening) at  $T_{\text{eff}} \gtrsim 20000$  K (cf. Figs. 6d–6f).

### 6.2. Non-LTE Corrected Abundances

Since non-LTE corrections are appreciably dependent upon [P/H], it is necessary to adopt a correction corresponding to an adequate [P/H] consistent with the final non-LTE abundance. Therefore, we proceed as follows.

First, three kinds of non-LTE abundances are derived from  $W_{6043}$  ( $A_{-1}^N$ ,  $A_0^N$ , and  $A_{+1}^N$ , corresponding to [P/H] = -1, 0, and +1, respectively) by using three sets of departure coefficients prepared for each star (cf. Sect. 5.2). These three non-LTE abundances are sufficient to express  $A^N$  by a second-order polynomial in terms of  $x$  ( $\equiv$  [P/H]) as

$$A^N = ax^2 + bx + c, \quad (2)$$

where  $a$ ,  $b$ , and  $c$  are known coefficients. Meanwhile, according to the definition,

$$A^N = x + 5.45. \quad (3)$$

Combining Eqs. (2) and (3), we have

$$ax^2 + bx + c = x + 5.45. \quad (4)$$

Let us denote the solution of Eq. (4) as  $x_*$  (which of two solutions should be adopted is self-evident), from which we obtain  $A_*^N (= x_* + 5.45)$  and  $\Delta_* (= A_*^N - A^L)$  as the final non-LTE abundance and non-LTE correction.

Such derived  $\Delta_*$  values are plotted against  $T_{\text{eff}}$  in Fig. 7b (black filled circles), where  $\Delta_{-1}$  (blue),  $\Delta_0$  (green), and  $\Delta_{+1}$  (red) are also overplotted by open symbols for comparison. Likewise, the final non-LTE abundances ( $A_*^N$ ) are shown against  $T_{\text{eff}}$  in Fig. 7c.

## 7. Phosphorus Abundances of B-type Stars

It is apparent from Fig. 7c that the P abundances of the program stars are divided into two groups: (i) late B-type chemically peculiar stars which exhibit conspicuous overabundances systematically increasing from  $A^N \sim 6$  ( $T_{\text{eff}} \sim 10000$  K) to  $A^N \sim 7$  ( $T_{\text{eff}} \sim 16000$  K), and (ii) normal early-to-late B-type stars ( $10000 \lesssim T_{\text{eff}} \lesssim 22000$  K) which show rather similar P abundances irrespective of  $T_{\text{eff}}$ . These two groups of stars are separately discussed below.

### 7.1. P-rich Peculiar Stars

The former P-enhanced group mostly consists of non-magnetic late B-type chemically peculiar stars (HgMn stars), which are known to show considerable overabundance of P. Nevertheless, P-rich stars and those classified as HgMn peculiar stars are not strictly equivalent but some exceptions do exist (P-strong stars classified as normal or P-weak HgMn stars).

The tendency observed in Fig. 7c (P is overabundant in HgMn stars and its anomaly increases with  $T_{\text{eff}}$ ) is actually a reconfirmation of the trend shown in

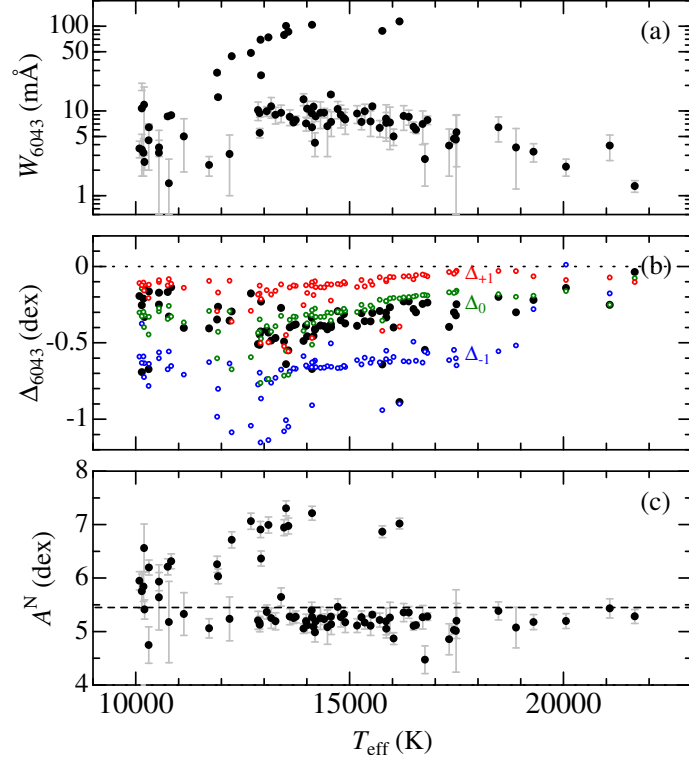


Fig. 7. The equivalent widths (same as in Fig. 4a) of the P II 6043 line, the finally adopted non-LTE corrections, and the corresponding non-LTE abundances for each of the program stars are plotted by black filled circles against  $T_{\text{eff}}$  in panels (a), (b), and (c), respectively. In panel (b), the original non-LTE corrections ( $\Delta_{-1}$ ,  $\Delta_0$ , and  $\Delta_{+1}$ ; corresponding to  $[P/H] = -1, 0,$  and  $+1$ ), from which the final  $\Delta$  was derived, are also depicted for comparison by open circles (colored in blue, green, and red, respectively). The error bars attached to the symbols in panels (a) and (c) are the same as in Figs. 4a and 4b.

Fig. 4 of Ghazaryan & Alecian (2016), though the extent of overabundance seen in their figure ( $[P/H] \sim +2$  at  $T_{\text{eff}} \sim 14000$  K) appears to be somewhat overestimated by  $\sim +0.5$  dex in comparison with Fig. 7c, which is presumably due to their neglect of non-LTE corrections.

It should be noted, however, that P abundances derived by using the conventional model atmosphere (1D plane-parallel model with vertically changing physical variables but homogeneous abundances) are of limited significance in the present case of HgMn stars, because the chemical composition of P is likely to be stratified in their atmospheres (i.e., increasing with height) due to the element segregation process as indicated by recent studies (see, e.g., Catanzaro et al. 2016, Ndiaye et al. 2018, Alecian & Stift 2019).

## 7.2. Superficially Normal B-type Stars

We are now to discuss the photospheric P abundances of normal B-type stars, which should retain the composition of galactic gas from which they were formed.

As long as LTE abundances are concerned, their  $A^L$  values almost distribute around the solar abundance ( $A_{\odot} = 5.45$ ) but exhibit a  $T_{\text{eff}}$ -dependent trend at  $T_{\text{eff}} \lesssim 16000$  K ( $dA^L/dT_{\text{eff}} \sim 0.1$  dex/1000 K) as shown in Fig. 4c.

However, since the non-LTE corrections ( $\Delta$ ) also have a systematic gradient with  $T_{\text{eff}}$  just in the inverse sense (Fig. 7b), the non-LTE abundances ( $A^N$ ) turn out to be almost independent upon  $T_{\text{eff}}$  (Fig. 7c), accomplishing a reasonable homogeneity. An inspection of Fig. 7c suggests that the demarcation line dividing the two groups may be set at  $\sim 5.7$ . Then, those 61 stars satisfying the criterion  $A^N < 5.7$  are regarded as normal B stars, for which the mean abundance is calculated as  $\langle A^N \rangle = 5.20$  (standard deviation is  $\sigma = 0.18$ ).

Here, we are confronted with a somewhat puzzling problem if this result is compared with the reference solar abundance of  $A_{\odot} = 5.45$ . That is, P abundances of young B-type stars (representing the gas composition at the time of some  $\sim 10^7 - 10^8$  yr ago) are by  $\sim 0.2-0.3$  dex “lower” than that of the Sun (formed  $\sim 4.6 \times 10^9$  yr ago). This may suggest that P abundance of galactic gas has “decreased” with time, which apparently contradicts the standard concept of chemical evolution in the Galaxy (elements are synthesized and expelled by stars, by which gas is chemically enriched with the lapse of time).

Given that P abundances were determined based only on one line (P II 6043), whether its transition probability is credible or not may be worth checking, because it directly affects the result. The adopted  $\log gf = +0.442$  for this line (taken from VALD) was obtained by Dr. Kurucz in 2012 based on the new observed data of P II levels, by which the previous Kurucz & Bell’s (1995) value of +0.384 was somewhat revised. This VALD value is also quite consistent with the data (+0.42) of Wiese et al. (1969), which is also included in the database of NIST (National Institute of Standards and Technology). Therefore, it is unlikely that our  $A^N$  results are significantly underestimated due to the use of an erroneous  $gf$  value.

Another possibility is that the actual solar P abundance might be lower than the currently believed value ( $A_{\odot} \sim 5.4-5.5$ ). This problem is separately focused upon in Appendix A. As discussed therein (cf. Sect. A5), although a possibility can not be ruled out that  $A_{\odot}$  could be somewhat reduced by  $\lesssim 0.1-0.2$  dex (i.e., down to  $\sim 5.3$ ), since uncertainties are still involved with P I line formation calculations (e.g., H I collision rates, treatment of 3D effect), there is no convincing reason for such a downward revision of  $A_{\odot}$ . Moreover, if the solar photospheric P abundance were to be appreciably changed, another problem of discrepant  $A_{\odot}$  from  $A_{\text{meteorite}}$  would newly emerge, because a good agreement has already been accomplished between these two (Asplund et al. 2009).

Therefore, frankly accepting the result of the analysis, we conclude that the phosphorus abundances of B-type stars ( $\langle A^N \rangle$ ) are systematically lower than that of the Sun ( $A_{\odot}$ ) by  $\sim 0.2-0.3$  dex. The cause for such a puzzling discrepancy (apparently contradicting the scenario of galactic chemical evolution) would be worth further earnest investigation. Meanwhile, follow-up studies by other researchers

are also desirably awaited for an independent check of this observational finding.

## 8. Summary and Conclusion

Recently, special attention is being focused on the abundance of phosphorus in the universe, mainly because of its astrobiological importance as a key element for life. For example, whether or not a sufficient amount of P (required for the rise of life) remains on the surface of a planet depends critically upon the primordial P abundance of the material, from which a star and the associated planetary system were formed.

Stimulated by such increasing interest, a number of spectroscopic studies intending to establish stellar P abundances have been published lately. These P-specific investigations are directed to late-type (FGK-type) stars of lower mass (around  $\sim 1M_{\odot}$ ), which are generally long-lived and thus retain the information of P composition in comparatively earlier time of the Galaxy ( $\sim 10^9 - 10^{10}$  yr ago) when they were formed.

However, little efforts have been made so far to comprehensive P abundance determinations of young hotter stars, such as B-type stars of  $\sim 3-10 M_{\odot}$ , which reflect the gas composition of the Galaxy in the more recent past (several times  $\sim 10^7 - 10^8$  yr ago). This is presumably because P lines of sufficient strength usable as abundance indicators are scarce. Actually, many of those B-type stars for which such determinations were done are P-rich chemically peculiar stars (HgMn stars), while the number of normal B-type stars with known P abundances is quite limited.

Thus, motivated by the necessity of clarifying the behavior of phosphorus in hotter stars of higher mass, P abundances of  $\sim 80$  apparently bright sharp-lined early-to-late B-type stars on the upper main sequence were determined from the P II 6043.084 Å line (the strongest P II line in the optical region), with an aim of getting information on the composition of this element in the young galactic gas in comparison with the abundance of the older Sun (age of  $4.6 \times 10^9$  yr).

A special emphasis was placed upon taking into account the non-LTE effect based on extensive statistical-equilibrium calculations on P II atoms, since the assumption of LTE was assumed in all the previous P abundance determinations.

Regarding the procedures of analysis, a spectrum-fitting was first applied to the wavelength region comprising the P II 6043 line, and its equivalent width ( $W_{6043}$ ) was then derived from the fitting-based abundance solution for each star. Finally, non-LTE abundance/correction as well as possible error were evaluated from such established  $W_{6043}$ . An inspection of the resulting P abundances revealed that the program stars are divided into two groups.

The first group is those showing a considerable overabundance of P (supersolar by  $\sim 0.5-1.5$  dex), the extent of which progressively increases with  $T_{\text{eff}}$ . These P-rich stars are observed at  $T_{\text{eff}} \lesssim 16000$  K (late B-type) and mostly belong to chemically peculiar stars of HgMn-type.



The second group consists of normal B-type stars, whose P abundances are comparatively homogeneous without such a prominent P anomaly as in the first group. However, different trends are observed between the LTE and non-LTE cases. (i) Though the LTE abundances tend to distribute around the solar value, they show a slight gradient (i.e., increasing with a decrease in  $T_{\text{eff}}$  at  $T_{\text{eff}} \gtrsim 16000$  K). (ii) Meanwhile, this systematic trend disappears in the non-LTE abundances which are satisfactorily uniform, because of the cancellation due to the  $T_{\text{eff}}$ -dependent negative non-LTE corrections (amounting to  $\sim 0.1$ – $0.5$  dex).

This  $T_{\text{eff}}$ -independent nature seen in the non-LTE abundances of normal B stars suggests that they represent the P composition of the galactic gas at the time when these young stars were born (some  $\sim 10^7$ – $10^8$  yr ago). One puzzling problem is, however, that these non-LTE abundances (around  $\sim 5.2$ ) are appreciably lower than the P abundance of the Sun (formed  $\sim 4.6 \times 10^9$  yr ago) by  $\sim 0.2$ – $0.3$  dex, which means that the galactic gas composition of P has decreased with time in contradiction to the concept of chemical evolution.

Although other possibilities (e.g., error in the adopted  $gf$  value of P II 6043 line?, inadequacy in the current solar P abundance?) were also examined, they do not seem to be so likely. It may thus be concluded that the discrepancy of P abundance between the Sun and B-type stars really exists, the cause of which should be further investigated.

**Acknowledgements.** This investigation has made use of the SIMBAD database, operated by CDS, Strasbourg, France, and the VALD database operated at Uppsala University, the Institute of Astronomy RAS in Moscow, and the University of Vienna.

## REFERENCES

- Alecian, G., & Stift, M. J. 2019, *MNRAS*, **482**, 4519.
- Allen, C. S., 1998, *Abundance analysis of normal and mercury-manganese type late-B stars from optical spectra* (PhD Thesis: University College London) [<https://discovery.ucl.ac.uk/id/eprint/10097529/>].
- Anders, E., & Grevesse, N. 1989, *Geochim. Cosmochim. Acta*, **53**, 197.
- Asplund, M., Grevesse, N., & Sauval, A. J., 2005, in *Cosmic Abundances as Records of Stellar Evolution and Nucleosynthesis*, ASP Conf. Ser., **336**, 25.
- Asplund, M., Grevesse, N., Sauval, A. J., & Scott, P. 2009, *ARA&A*, **47**, 481.
- Bekki, K., & Tsujimoto, T. 2024, *ApJL*, **967**, L1.
- Biémont, E., Martin, F., Quinet, P., & Zeippen, C. J. 1994, *A&A*, **283**, 339.
- Caffau, E., Steffen, M., Sbordone, L., Ludwig, H.-G., & Bonifacio, P. 2007, *A&A*, **473**, L9.
- Catanzaro, G., Giarrusso, M., Leone, F., Munari, M., Scialia, C., Sparacello, E., & Scuderi, S. 2016, *MNRAS*, **460**, 1999.
- Cayrel, R. 1988, in *The Impact of Very High S/N Spectroscopy on Stellar Physics, Proceedings of IAU Symposium 132*, ed. G. Cayrel de Strobel, M. Spite (Kluwer, Dordrecht), p.345.

- Fossati, L., Ryabchikova, T., Bagnulo, S., Alecian, E., Grunhut, J., Kochukhov, O., & Wade, G. 2009, *A&A*, **503**, 945.
- Ghazaryan, S., & Alecian, G. 2016, *MNRAS*, **460**, 1922.
- Golriz, S. S., & Landstreet, J. D. 2017, *MNRAS*, **466**, 1597.
- Hinkel, N. R., Hartnett, H. E., & Young, P. 2020, *ApJL*, **900**, L38.
- Hoffleit, D. & Jaschek, C., 1991, *The Bright Star Catalogue, 5th revised edition*, (New Haven, Conn.: Yale University Observatory).
- Kurucz, R. L. 1993, *Kurucz CD-ROM*, No. 13 (Harvard-Smithsonian Center for Astrophysics).
- Kurucz, R. L., & Bell, B. 1995, *Kurucz CD-ROM*, No. 23 (Harvard-Smithsonian Center for Astrophysics).
- Lejeune, T., & Schaerer, D. 2001, *A&A*, **366**, 538.
- Lodders, K., Palme, H., & Gail, H.-P. 2009, *Solar System, Landolt-Börnstein - Group VI Astronomy and Astrophysics, Volume 4B*, p. 712 (Springer, Berlin).
- Maas, Z. G., Hawkins, K., Hinkel, N. R., Cargile, P., Janowiecki, S., & Nelson, T. 2022, *AJ*, **164**, 61.
- Moore, C. E., 1959, *A multiplet Table of Astrophysical Interest: NBS Technical Note No. 36, Reprinted Version of the 1945 edition* (U. S. Department of Commerce, Washington).
- Nahar, S. N., Hernández, E. M., Hernández, L., et al. 2017, *JQSRT*, **187**, 215.
- Ndiaye, M. L., LeBlanc, F., & Khalack, V. 2018, *MNRAS*, **477**, 3390.
- Niemczura, E., Morel, T., & Aerts, C. 2009, *A&A*, **506**, 213.
- Peters, G. J., & Aller, L. H. 1970, *ApJ*, **159**, 525.
- Peters, G. J., & Polidan, R. S., 1985, *Proc. IAU Symp. 111, Calibration of Fundamental Stellar Quantities* (Reidel, Dordrecht), p. 417.
- Pintado, O. I., & Adelman, S. J. 1993, *MNRAS*, **264**, 63.
- Przybilla, N., Butler, K., Becker, S. R., & Kudritzki, R. P. 2006, *A&A*, **445**, 1099.
- Ryabchikova, T., Piskunov, N., Kurucz, R. L., Stempels, H. C., Heiter, U., Pakhomov, Yu., & Barklem, P. S. 2015, *Phys. Scr.*, **90**, 054005.
- Sadakane, K., & Nishimura, M. 2022, *PASJ*, **74**, 298.
- Steenbock, W., & Holweger, H. 1984, *A&A*, **130**, 319.
- Takeda, Y. 1991, *A&A*, **242**, 455.
- Takeda, Y. 2023, *Acta Astron.*, **73**, 35.
- Takeda, Y., Kambe, E., Sadakane, K., & Masuda, S. 2010, *PASJ*, **62**, 1239 (Paper I).
- Takeda, Y., Kawanomoto, S., & Ohishi, N. 2014, *PASJ*, **66**, 23 (Paper II).
- Tayal, S. S. 2004, *J. Phys. B: At. Mol. Opt. Phys.*, **37**, 3593.
- Wiese, W. L., Smith, M. W., & Miles, B. M. 1969, *Atomic transition probabilities, Vol. II: Sodium through calcium - A critical data compilation, in Nat. Stand. Ref. Data Ser., NSRDS-NBS 22* (U.S. Government Printing Office, Washington, D.C.).

## Appendix A: On the Solar Photospheric Abundance of Phosphorus

### A1. Literature Values of Solar P Abundance

Regarding the phosphorus abundance in the solar photosphere (usually derived from P I lines in the *Y*- or *H*-band of the near-IR region), not a few spectroscopic studies have been published over the past half century, in which rather similar  $A_{\odot}$  values of  $\simeq 5.4$ – $5.5$  are reported. See Table 2 of Caffau et al. (2007) for a summary of 8 values (5.43, 5.45, 5.45, 5.45, 5.49, 5.45, 5.36, and 5.46) published before 2007. Thereafter, Asplund et al. (2009) presented a revised value of  $A_{\odot} = 5.41$ . The Anders & Grevesse's (1989) value of  $A_{\odot} = 5.45$  adopted in this paper (cf. footnote 3) is almost the same as the mean of these values.

However, all these determinations were done with the assumption of LTE, given the lack of information regarding the non-LTE effect on the P I lines so far. Therefore, non-LTE calculations for neutral phosphorus were newly carried out in order to elucidate how and whether the non-LTE corrections are important in P abundance determinations for the Sun. In addition, how this effect would depend upon the atmospheric parameters is also briefly examined in scope of application to late-type stars in general.

### A2. Atomic Model

The adopted model atom of P I comprises 56 terms (up to  $3s^2 3p^2 5d^4 D$  at  $79864 \text{ cm}^{-1}$ ) and 761 radiative transitions, which was constructed in a similar manner to the case of P II described in Sect. 5. The contribution of P II was taken into account in the number conservation of total P atoms.

Regarding the photoionization cross section, Tayal's (2004) theoretically calculated data were adopted for the lowest three terms ( $^4S^{\circ}$ ,  $^2D^{\circ}$ ,  $^2P^{\circ}$ ; read from Fig. 1–3, Fig. 9, and Fig. 10 of his paper), while the hydrogenic approximation was assumed for the other terms.

As to the collisional rates, the recipe described in Sect. 3.1.3 of Takeda (1991) was basically followed. The collision rates due to neutral hydrogen atoms (which are important in late-type stars but subject to large uncertainties) were computed by Steenbock & Holweger's (1984) formula (based on the classical Drawin's cross section), which can be further multiplied by a correction factor ( $k$ ) if necessary. Although we adopt  $k = 1$  (use of classical formula unchanged) as the standard choice, a special case of  $k = 10^{-3}$  (considerably reduced to a negligible level) was also tried in order to see its importance.

### A3. Non-LTE Effect on P I 10581 Line in FGK-type Stars

First, the calculations were done for 10 solar-metallicity models (ATLAS9 models by Kurucz 1993) resulting from combinations of ( $T_{\text{eff}} = 4500, 5000, 5500, 6000, 6500 \text{ K}$ ) and ( $\log g = 2.0, 4.0$ ), while assuming  $\xi = 2 \text{ km s}^{-1}$  and  $[P/H] =$

0 ( $A = 5.45$ ). The runs of  $I_0^{\text{NLTE}}/I_0^{\text{LTE}}$  and  $S_L/B$  with depth for the transition corresponding to P I 10581.58 line (representative P I line in the near-IR region) are shown in Fig. 8, while Fig. 9 displays how  $W_{10581}$  (equivalent widths calculated in LTE and non-LTE; upper panel (a)) as well as  $\Delta_{10581}$  (non-LTE correction; lower panel (b)) depend upon  $T_{\text{eff}}$  and  $\log g$ . The following characteristics are read from these figures.

- The line is generally intensified by the non-LTE effect ( $W^{\text{N}} > W^{\text{L}}$  and  $\Delta < 0$ ; cf. Fig. 9), because both  $I_0^{\text{NLTE}}/I_0^{\text{LTE}} > 1$  and  $S_L/B < 1$  (cf. Fig. 8) act in the direction of line strengthening.
- This non-LTE effect becomes progressively larger with an increase in  $T_{\text{eff}}$  and with a decrease in  $\log g$  (Fig. 9b).
- How the neutral hydrogen collision is treated has an appreciable impact on the non-LTE correction. If the standard value of H I collision is practically neglected by a drastic reduction ( $k = 10^{-3}$ ),  $|\Delta|$  increases by  $\sim 0.1$ – $0.2$  dex (Fig. 9b).
- In summary, non-LTE corrections had better be taken into account in P abundance determinations from P I lines for FGK stars, especially for those of comparatively higher  $T_{\text{eff}}$  or lower  $\log g$ , for which significant negative corrections amounting to several tenths dex may be expected.

#### A4. Reanalysis of Solar P I Lines

Then, statistical equilibrium calculation was done for Kurucz's (1993) ATLAS9 solar model atmosphere ( $T_{\text{eff}} = 5780$  K,  $\log g = 4.44$ , solar metallicity) with  $[P/H] = 0.0$ , in order to reanalyze the solar P I lines by taking into account the non-LTE effect. The basic data for the solar equivalent widths and  $\log gf$  values of 15 P I lines were taken from Table 3 of Biémont et al. (1994), which are the disk-center values measured from Jungfraujoch Atlas ( $W_{\lambda}^{\text{d.c.}}$ ) and transition probabilities based on their refined calculations. Regarding the solar microturbulence, a reasonable value of  $\xi_{\odot} = 1$  km s $^{-1}$  was adopted as often assumed. The resulting P abundances and non-LTE corrections are summarized in Table 2, from which the following conclusions can be drawn.

The extents of (negative) non-LTE corrections are only a few hundredths dex ( $k = 1$  case) and thus not particularly important, though  $|\Delta|$  may somewhat increase further by  $\sim 0.1$  if H I collision is neglected ( $k = 10^{-3}$ ). This is mainly due to the high-gravity nature of the Sun ( $\log g = 4.44$ ) as a dwarf, since  $|\Delta|$  appreciably decreases with an increase in  $\log g$  (cf. Fig. 9b).<sup>9</sup> Therefore, the speculation

<sup>9</sup>Actually,  $|\Delta|$  in this case (disk-center intensity spectrum) is somewhat smaller than that obtained by an interpolation/extrapolation of Fig. 9b (calculated for the flux spectrum), because the non-LTE effect becomes less significant for the former case of deeper-forming lines than the latter.

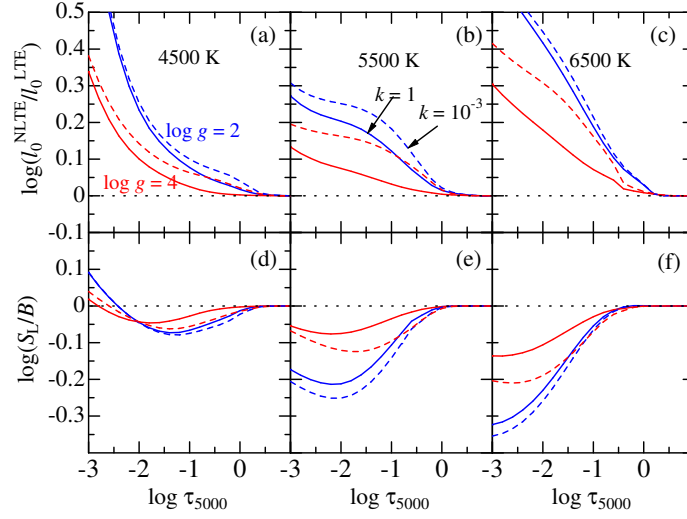


Fig. 8. The non-LTE-to-LTE line-center opacity ratio (upper panels (a)–(c)) and the ratio of the line source function ( $S_L$ ) to the local Planck function ( $B$ ) (lower panels (d)–(f)) for the P I  $4s\ ^4P^\circ - 4s\ ^4D$  transition (corresponding to P I 10581 line) of multiplet 1, plotted against the continuum optical depth at 5000 Å. Shown here are the calculations done with  $\xi = 2\text{ km s}^{-1}$  and the solar P abundance ( $[P/H] = 0$ ) on the solar-metallicity models of  $T_{\text{eff}} = 4500\text{ K}$  (left panels (a), (d)), 5500 K (middle panels (b), (e)), and 6500 K (right panels (c), (f)). For two surface gravities of  $\log g = 2$  and 4. At each panel, the results for different treatment of neutral hydrogen collisions ( $k = 1$  and  $10^{-3}$ ) are discriminated by line-types (solid and dashed lines), while those of  $\log g = 2.0$  and 4.0 are depicted by different colors (blue and red, respectively).

addressed by Asplund et al. (2009) “departures from LTE are not expected to be significant for P” (based on an analogy with the S I case) may be regarded as reasonable.

The mean P abundances averaged over 15 lines are  $\langle A^L \rangle = 5.43$  (LTE abundance),  $\langle A_{k=1}^N \rangle = 5.40$  (non-LTE abundance for  $k = 1$ ), and  $\langle A_{k=10^{-3}}^N \rangle = 5.31$  (non-LTE abundance for  $k = 10^{-3}$ ), where the standard deviation is  $\sigma = 0.11$  for all the three cases. This  $\langle A^L \rangle$  (5.43) is reasonably consistent with Biémont et al.’s (1994) result of 5.45 (obtained by using the same lines with the same  $W_\lambda^{\text{d.c.}}$  and  $\log gf$ ). According to the standard non-LTE abundance of 5.40 ( $\langle A_{k=1}^N \rangle$ ) obtained here, we may state that the previously reported results of solar P abundance (cf. Sect. A1) can not be significantly revised even when the non-LTE correction (a few hundredths dex) is taken into account.

#### A5. Is Downward Revision of $A_\odot$ Possible?

In view of discrepancy between the P abundances of normal B-type stars and that of the Sun (the former being systematically lower than the latter by  $\sim 0.2$ – $0.3$  dex) discussed in Sect. 7.2, some discussion about whether the actual  $A_\odot$  could be lower than the currently accepted value may be in order.

Neglecting the H I collision would further reduce  $A^N$  by  $\sim 0.1$  dex down to  $\sim 5.3$ . However, there is no justification for such a drastic reduction of the classical

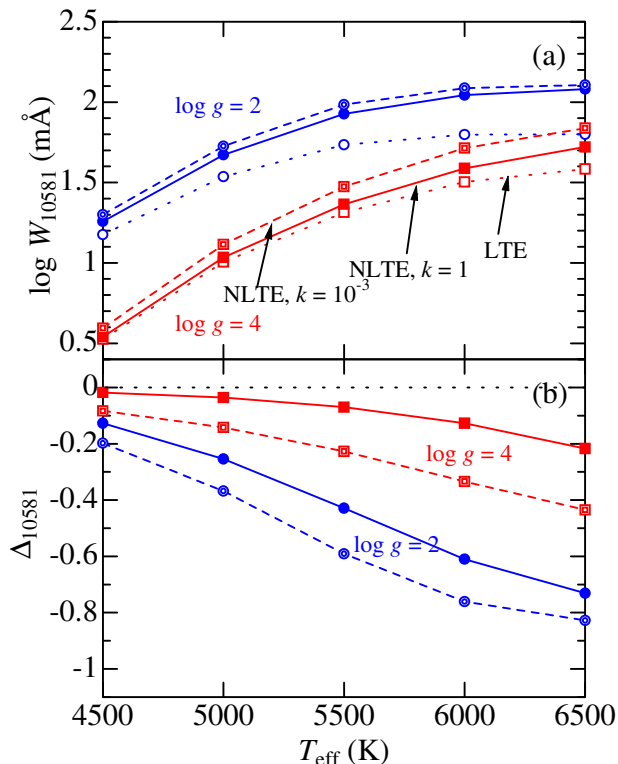


Fig. 9. Theoretical equivalent widths ( $W$ ) calculated for the P I 10581 line and the corresponding non-LTE corrections are plotted against  $T_{\text{eff}}$ . In panel (a), the runs of  $W^{\text{L}}$  (LTE),  $W_{k=1}^{\text{N}}$  (non-LTE with  $k = 1$ ), and  $W_{k=10^{-3}}^{\text{N}}$  (non-LTE with  $k = 10^{-3}$ ) are depicted in dotted, solid, and dashed lines, respectively. Similarly, the runs of  $\Delta_{k=1}$  (solid lines) and  $\Delta_{k=10^{-3}}$  (dashed lines) are shown in panel (b). These calculations were done with the solar P abundance ( $[P/H] = 0.0$ ) on 10 solar metallicity models for two  $\log g$  (2 and 4) and five  $T_{\text{eff}}$  (4500, 5000, 5500, 6000, and 6500 K) values. The results for  $\log g = 2$  and 4 are depicted in blue and red, respectively.

rates for rather high-excitation P I lines under question.<sup>10</sup> Therefore, much can not be said about this possibility until more information of H I collision rates for P I is obtained (preferably based on up-to-date quantum-mechanical calculations).

Alternatively, it was once considered that inclusion of the 3D effect might reduce  $A_{\odot}$  by  $\lesssim 0.1$  dex, since Asplund et al. (2005) derived an appreciably lower value of  $A_{\odot} = 5.36$  by including the 3D-effect. However, such a low-scale result was not confirmed by Caffau et al.'s (2007) new 3D analysis which resulted in  $A_{\odot} = 5.46(\pm 0.04)$ , showing that the 3D correction is insignificant (only a few hundredths dex) for the solar P abundance determination. Thus, this possibility is not very prospective, either.

In any case, although a possibility of solar P abundance being reduced by

<sup>10</sup>Admittedly, such a situation does exist for the case of other lines. For example, it is known that neutral-hydrogen collision rates calculated by using the classical cross section are considerably overestimated for the resonance lines of alkali elements (e.g., Li I 6708 or K I 7699).

$\lesssim 0.1\text{--}0.2$  (i.e., down to  $\sim 5.3$ ) can not be excluded, the solar P abundance would then be discrepant from that of meteorite. That is, since the old  $A_{\text{meteorite}}(\text{P})$  value of  $5.57 \pm 0.04$  derived by Anders & Grevesse (1989) was revised by Asplund et al. (2009) as  $5.43 \pm 0.04$  (based on the data of CI carbonaceous chondrites taken from Lodders et al. 2009), a good agreement between  $A_{\text{meteorite}}$  and  $A_{\odot}$  is now accomplished. This consistency would break down if  $A_{\odot}$  were appreciably changed.

Table 1: Program stars and the results of the analysis.

HD#	HR#	star name	Sp.Type	$*T_{\text{eff}}$	$*\log g$	$\dagger v_e \sin i$	$W_{6043}$	$A^L$	$\Delta$	$A^N$	#S/N
(1)	(2)	(3)	(4)	(5)	(6)	(7)	(8)	(9)	(10)	(11)	(12)
[2006 October observations (early-to-late B-type stars)]											
029248	1463	v Eri	B2III	22651	3.58	46	...	...	...	...	450
000886	0039	$\gamma$ Peg	B2IV	21667	3.83	9	1.3	5.32	-0.04	5.28	730
035708	1810	114 Tau	B2.5IV	21082	4.09	26	3.9	5.68	-0.25	5.43	470
035039	1765	22 Ori	B2IV-V	20059	3.69	10	2.2	5.34	-0.14	5.20	460
042690	2205		B2V	19299	3.81	12	3.3	5.40	-0.22	5.18	470
032249	1617	$\psi$ Eri	B3V	18890	4.13	40	3.7	5.38	-0.30	5.07	500
034447	1731		B3IV	18480	4.10	9	6.4	5.58	-0.20	5.38	300
196035	7862		B3IV	17499	4.36	35	5.6	5.45	-0.25	5.20	300
043157	2224		B5V	17486	4.12	37	4.6	5.33	-0.32	5.01	210
160762	6588	t Her	B3IV	17440	3.91	7	4.7	5.33	-0.30	5.03	380
223229	9011		B3IV	17327	4.20	31	3.9	5.25	-0.40	4.86	390
176502	7179		B3V	16821	3.89	8	7.8	5.52	-0.24	5.28	340
041753	2159	v Ori	B3V	16761	3.90	28	2.7	5.02	-0.55	4.47	520
025558	1253	40 Tau	B3V	16707	4.29	41	7.0	5.51	-0.25	5.27	360
044700	2292		B3V	16551	4.21	5	6.0	5.42	-0.30	5.12	360
186660	7516		B3III	16494	3.57	9	6.5	5.38	-0.28	5.11	370
181858	7347		B3IVp	16384	4.19	17	8.5	5.58	-0.23	5.36	340
023793	1174	30 Tau	B3V+F5V	16264	4.15	46	8.7	5.59	-0.23	5.36	510
185330	7467		B5II-III	16167	3.77	4	113.4	7.91	-0.89	7.02	360
027396	1350	53 Per	B4IV	16028	3.91	15	5.0	5.27	-0.40	4.87	410
034798	1753		B3V	15943	4.27	37	7.3	5.53	-0.27	5.26	310
184171	7426	8 Cyg	B3IV	15858	3.54	27	7.2	5.39	-0.34	5.05	420
198820	7996		B3III	15852	3.86	32	8.1	5.49	-0.30	5.19	300
030122	1512		B5III	15765	3.72	15	87.8	7.51	-0.64	6.87	310
020756	1005	$\tau^1$ Ari	B5IV	15705	4.43	18	6.3	5.51	-0.29	5.21	460
037971	1962		B3IVp	15532	3.63	9	11.3	5.62	-0.31	5.31	470
026739	1312		B5IV	15490	3.92	31	7.5	5.47	-0.36	5.11	360
209008	8385	18 Peg	B3III	15353	3.50	20	9.9	5.53	-0.36	5.17	340
028375	1415		B3V	15278	4.30	19	7.4	5.57	-0.31	5.27	430
011415	0542	$\epsilon$ Cas	B3III	15174	3.54	42	9.3	5.50	-0.39	5.11	580
147394	6092	$\tau$ Her	B5IV	14898	4.01	30	7.9	5.55	-0.37	5.17	480
019268	0930		B5V	14866	4.24	17	8.2	5.64	-0.31	5.33	410
189944	7656		B4V	14793	4.01	35	9.0	5.62	-0.35	5.27	320
181558	7339		B5V	14721	4.15	14	10.5	5.75	-0.29	5.46	300
224990	9091	$\zeta$ Scl	B4III	14569	3.99	35	7.4	5.53	-0.40	5.14	350
175156	7119		B5II	14561	2.79	12	15.6	5.66	-0.38	5.28	460
199578	8022		B5V	14480	4.02	27	6.6	5.49	-0.41	5.08	230
209419	8403		B5III	14404	3.82	16	9.5	5.62	-0.39	5.23	400
202753	8141	15 Aqr	B5V	14318	3.84	40	9.5	5.64	-0.39	5.25	360
023300	1141		B6V	14207	3.84	19	8.6	5.59	-0.40	5.19	540
182255	7358	3 Vul	B6III	14190	4.29	28	4.2	5.40	-0.41	4.99	550
041692	2154		B5IV	14157	3.19	28	11.2	5.54	-0.46	5.09	490
049606	2519	33 Gem	B7III	14121	3.82	19	103.6	7.89	-0.67	7.21	360
212986	8554		B5III	14121	4.27	20	6.4	5.61	-0.34	5.27	340
016219	0760		B5V	14113	4.06	23	9.4	5.73	-0.33	5.40	350
188892	7613	22 Cyg	B5IV	14008	3.38	30	10.6	5.58	-0.46	5.12	390
206540	8292		B5IV	13981	4.01	13	7.1	5.58	-0.39	5.19	280
191243	7699		B5Ib	13923	2.50	28	13.7	5.54	-0.49	5.05	410
210424	8452	38 Aqr	B7III	13740	3.99	12	7.8	5.66	-0.38	5.28	440
201888	8109		B7III	13689	4.01	5	7.3	5.64	-0.38	5.25	350
011857	0561		B5III	13600	3.88	20	8.5	5.68	-0.40	5.28	430
053244	2657	$\gamma$ CMa	B8II	13467	3.42	36	78.4	7.43	-0.49	6.94	510
155763	6396	$\zeta$ Dra	B6III	13397	4.24	41	9.5	5.92	-0.27	5.64	550
173117	7035		B5:V	13267	3.63	22	9.0	5.66	-0.47	5.19	400
017081	0811	$\pi$ Cet	B7V	13063	3.72	20	9.9	5.78	-0.42	5.37	510
023408	1149	20 Tau	B8III	12917	3.36	30	69.0	7.33	-0.43	6.91	610
196426	7878		B8IIIp	12899	3.89	6	5.5	5.57	-0.45	5.13	320
179761	7287	21 Aql	B8II-III	12895	3.46	16	9.4	5.68	-0.51	5.16	490
011529	0548	$\omega$ Cas	B8III	12858	3.43	30	10.2	5.72	-0.51	5.21	460
178065	7245		B9III	12243	3.49	4	44.1	7.01	-0.29	6.71	190
038899	2010	134 Tau	B9IV	10774	4.02	26	1.4	5.51	-0.33	5.18	460
043247	2229	73 Ori	B9II-III	10301	2.39	33	4.5	5.42	-0.67	4.75	400
209459	8404	21 Peg	B9.5V	10204	3.53	3	2.5	5.74	-0.33	5.41	360
181470	7338		A0III	10085	3.92	2	3.6	6.14	-0.19	5.95	200



Table 1: (Continued.)

HD#	HR#	star name	Sp.Type	* $T_{\text{eff}}$	* $\log g$	$\dagger v_e \sin i$	$W_{6043}$	$A^L$	$\Delta$	$A^N$	#S/N
(1)	(2)	(3)	(4)	(5)	(6)	(7)	(8)	(9)	(10)	(11)	(12)
[2012 May observations (late B-type stars)]											
098664	4386	$\sigma$ Leo	B9.5V s	10194	3.75	62	11.8	6.70	-0.14	6.56	390
130557	5522		B9VSi:Cr:	10142	3.85	55	10.7	6.69	-0.12	6.57	260
079158	3652	36 Lyn	B8IIIpMn	13535	3.72	46	...	...	...	...	230
106625	4662	$\gamma$ Crv	B8IIIpHgMn	11902	3.36	37	28.2	6.61	-0.35	6.26	740
150100	6184	16 Dra	B9.5Vn	10542	3.84	36	3.2	5.89	-0.25	5.64	320
197392	7926		B8II-III	13166	3.46	30	11.3	5.74	-0.49	5.25	280
198667	7985	5 Aqr	B9III	11125	3.42	26	5.0	5.73	-0.40	5.33	220
202671	8137	30 Cap	B8III	13566	3.36	25	85.7	7.52	-0.55	6.97	220
193432	7773	v Cap	B9.5V	10180	3.91	24	3.2	6.05	-0.21	5.84	430
161701	6620		B9pHgMn	12692	4.04	20	48.2	7.24	-0.18	7.06	310
077350	3595	v Cnc	A0pSi	10141	3.68	20	3.5	6.01	-0.25	5.75	310
129174	5475	$\pi^1$ Boo	B9pMnHgSi	12929	4.02	16	26.3	6.60	-0.23	6.36	370
201433	8094		B9VpSi	12193	4.24	15	3.1	5.59	-0.35	5.24	190
144206	5982	v Her	B9III	11925	3.79	12	14.5	6.30	-0.26	6.03	450
145389	6023	$\phi$ Her	B9p:Mn:	11714	4.02	11	2.3	5.47	-0.41	5.06	490
190229	7664		B9pHgMn	13102	3.46	10	73.6	7.43	-0.43	6.99	280
149121	6158	28 Her	B9.5III	10748	3.89	10	8.6	6.38	-0.17	6.21	420
078316	3623	$\kappa$ Cnc	B8IIIpMn	13513	3.85	8	100.7	7.94	-0.64	7.30	290
089822	4072		A0pSiSr:Hg:	10307	3.89	5	6.4	6.36	-0.16	6.20	400
143807	5971	t CrB	A0p:Hg:	10828	4.06	4	8.9	6.45	-0.14	6.31	470
193452	7775		A0III	10543	4.15	3	3.7	6.11	-0.17	5.93	170

(1) Henry Draper Catalogue number. (2) Bright Star Catalogue number (Hoffleit & Jaschek 1991). (3) Star name in the constellation. (4) Spectral type (taken from Hoffleit & Jaschek 1991). (5) Effective temperature (in K). (6) Logarithmic surface gravity (in  $\text{cm s}^{-2}/\text{dex}$ ). (7) Projected rotational velocity (in  $\text{km s}^{-1}$ ). (8) Equivalent width of P II 6043 line (in mÅ). (9) P abundance in LTE (in dex). (10) Non-LTE correction (in dex). (11) P abundance in non-LTE (in dex). (12) Signal-to-noise ratio.

The first part present the data of 64 early-to-late B stars (observed in 2006 October), followed by the second part for 21 late B-type stars (observed in 2012 May). The former is arranged in the descending order of  $T_{\text{eff}}$  while the latter is in the descending order of  $v_e \sin i$ , in order to keep consistency with the corresponding original papers (Paper I and Paper II).

\* Determined from color indices of Strömgren's  $uvby\beta$  photometry (cf. Sect. 3).

$\dagger$  Determined from the fitting analysis around  $\sim 6150\text{--}6160$  Å region (cf. Paper I and Paper II).

# Mean of the results measured from five segments in the neighborhood of the P II 6043 line.

Table 2: Non-LTE analysis of solar photospheric P abundances.

Mult. (1)	Transition (2)	* $\lambda$ (3)	* $\chi_{\text{low}}$ (4)	† $\log gf$ (5)	† $W_{\lambda}^{\text{d.c.}}$ (6)	$A^{\text{L}}$ (7)	$A_{k=1}^{\text{N}}$ (8)	$\Delta_{k=1}$ (9)	$A_{k=10^{-3}}^{\text{N}}$ (10)	$\Delta_{k=10^{-3}}$ (11)
3	4s <sup>4</sup> P <sub>5/2</sub> –4p <sup>4</sup> S <sub>3/2</sub>	9525.741	6.985	–0.100	7.7	5.431	5.394	–0.037	5.297	–0.134
2	4s <sup>4</sup> P <sub>3/2</sub> –4p <sup>4</sup> P <sub>1/2</sub>	9750.748	6.954	–0.180	6.3	5.421	5.388	–0.033	5.296	–0.125
4	4s <sup>2</sup> P <sub>1/2</sub> –4p <sup>2</sup> P <sub>3/2</sub>	9790.194	7.176	–0.690	0.9	5.245	5.223	–0.022	5.149	–0.096
2	4s <sup>4</sup> P <sub>5/2</sub> –4p <sup>4</sup> P <sub>5/2</sub>	9796.828	6.985	+0.270	16.9	5.514	5.475	–0.039	5.372	–0.142
4	4s <sup>2</sup> P <sub>1/2</sub> –4p <sup>2</sup> P <sub>1/2</sub>	9903.671	7.176	–0.300	3.8	5.583	5.559	–0.024	5.482	–0.101
2	4s <sup>4</sup> P <sub>5/2</sub> –4p <sup>4</sup> P <sub>3/2</sub>	9976.681	6.985	–0.290	2.9	5.604	5.573	–0.031	5.485	–0.119
4	4s <sup>2</sup> P <sub>3/2</sub> –4p <sup>2</sup> P <sub>1/2</sub>	10204.716	7.213	–0.520	1.9	5.468	5.444	–0.024	5.369	–0.099
1	4s <sup>4</sup> P <sub>1/2</sub> –4p <sup>4</sup> D <sub>3/2</sub>	10511.588	6.936	–0.130	7.8	5.381	5.348	–0.033	5.252	–0.129
1	4s <sup>4</sup> P <sub>3/2</sub> –4p <sup>4</sup> D <sub>5/2</sub>	10529.524	6.954	+0.240	15.3	5.365	5.329	–0.036	5.224	–0.141
1	4s <sup>4</sup> P <sub>5/2</sub> –4p <sup>4</sup> D <sub>7/2</sub>	10581.577	6.985	+0.450	24.7	5.436	5.395	–0.041	5.279	–0.157
1	4s <sup>4</sup> P <sub>1/2</sub> –4p <sup>4</sup> D <sub>1/2</sub>	10596.903	6.936	–0.210	10.4	5.586	5.552	–0.034	5.453	–0.133
1	4s <sup>4</sup> P <sub>3/2</sub> –4p <sup>4</sup> D <sub>3/2</sub>	10681.406	6.954	–0.190	7.8	5.434	5.401	–0.033	5.305	–0.129
1	4s <sup>4</sup> P <sub>3/2</sub> –4p <sup>4</sup> D <sub>1/2</sub>	10769.511	6.954	–1.070	1.0	5.358	5.329	–0.029	5.240	–0.118
1	4s <sup>4</sup> P <sub>5/2</sub> –4p <sup>4</sup> D <sub>5/2</sub>	10813.141	6.985	–0.410	4.0	5.338	5.308	–0.030	5.216	–0.122
—	4s <sup>2</sup> P <sub>3/2</sub> –4p <sup>2</sup> D <sub>5/2</sub>	11183.240	7.213	+0.400	10.6	5.272	5.246	–0.026	5.170	–0.102

(1) Multiplet number (Moore 1959). (2) Spectroscopic designation of the lower and upper levels of the transition. (3) Air wavelengths (in Å). (4) Lower excitation potential (in eV). (5) Logarithm of the statistical weight of the lower level times the oscillator strength. (6) Solar equivalent widths at the disk center (in mÅ). (7) LTE abundance (in dex). (8) Non-LTE abundance for  $k = 1$  (in dex). (9) Non-LTE correction for  $k = 1$  (in dex). (10) Non-LTE abundance for  $k = 10^{-3}$  (in dex). (11) Non-LTE correction for  $k = 10^{-3}$  (in dex).

\* Taken from VALD (Ryabchikova et al. 2015).

† Taken from Biémont et al. (1994).